European Journal of Nuclear Medicine and Molecular Imaging (2022) 49:4145–4155
https://doi.org/10.1007/s00259-022-05893-8

ORIGINAL ARTICLE

Evaluation of pediatric malignancies using total-body PET/CT with half-dose [^{18}F]-FDG

Wanqi Chen[1,2] · Lei Liu[1,2] · Yinghe Li[1,2] · Shatong Li[1,2] · Zhijian Li[1,2] · Weiguang Zhang[1,2] · Xu Zhang[1,2] · Runze Wu[3] · Debin Hu[3] · Hongyan Sun[3] · Yun Zhou[3] · Wei Fan[1,2] · Yumo Zhao[1,2] · Yizhuo Zhang[1,4] · Yingying Hu[1,2]

Received: 12 March 2022 / Accepted: 25 June 2022 / Published online: 5 July 2022

Abstract

Purpose To explore the impact of a true half dose of [^{18}F]-FDG on image quality in pediatric oncological patients undergoing total-body PET/CT and investigate short acquisition times with half-dose injected activity.

Methods One hundred pediatric oncological patients who underwent total-body PET/CT using the uEXPLORER scanner after receiving a true half dose of [^{18}F]-FDG (1.85 MBq/kg) were retrospectively enrolled. The PET images were first reconstructed using complete 600-s data and then split into 300-s, 180-s, 60-s, 40-s, and 20-s duration groups (G600 to G20). The subjective analysis was performed using 5-point Likert scales. Objective quantitative metrics included the maximum standard uptake value (SUV_{max}), SUV_{mean}, standard deviation (SD), signal-to-noise ratio (SNR), and SNR_{norm} of the background. The variabilities in lesion SUV_{mean}, SUV_{max}, and tumor-to-background ratio (TBR) were also calculated.

Results The overall image quality scores in the G600, G300, G180, and G60 groups were 4.9 ± 0.2, 4.9 ± 0.3, 4.4 ± 0.5, and 3.5 ± 0.5 points, respectively. All the lesions identified in the half-dose images were localized in the G60 images, while 56% of the lesions could be clearly identified in the G20 images. With reduced acquisition time, the SUV_{max} and SD of the backgrounds were gradually increased, while the TBR values showed no statistically significant differences among the groups (all $p > 0.1$). Using the half-dose images as a reference, the variability in the lesion SUV_{max} gradually increased from the G180 to G20 images, while the lesion SUV_{mean} remained stable across all age groups. SNR_{norm} was highly negatively correlated with age.

Conclusion Total-body PET/CT with a half dose of [^{18}F]-FDG (1.85 MBq/kg, estimated whole-body effective dose: 1.76–2.57 mSv) achieved good performance in pediatric patients, with sufficient image quality and good lesion conspicuity. Sufficient image quality and lesion conspicuity could be maintained at a fast scanning time of 60 s with half-dose activity.

Keywords Pediatric · Total-body PET/CT · [^{18}F]-FDG · Low dose

Introduction

Positron emission tomography-computed tomography (PET/CT) plays an important role in tumor staging, restaging, and therapy response assessments [1, 2]. Compared with other

Wanqi Chen and Lei Liu contributed equally to this work

This article is part of the Topical Collection on Pediatric

✉ Yumo Zhao
zhaoym@sysucc.org.cn

✉ Yizhuo Zhang
zhangyzh@sysucc.org.cn

✉ Yingying Hu
huyy@sysucc.org.cn

[1] State Key Laboratory of Oncology in South China, Collaborative Innovation Center for Cancer Medicine, 651 Dongfengdong Road, Guangzhou 510060, Guangdong, China

[2] Department of Nuclear Medicine, Sun Yat-sen University Cancer Center, Guangzhou, Guangdong, China

[3] Central Research Institute, United Imaging Healthcare Group Co., Ltd, Shanghai, China

[4] Department of Pediatric Oncology, Sun Yat-sen University Cancer Center, Guangzhou, Guangdong, China

standard staging procedures, PET/CT shows improved sensitivities and specificities [3–5]. However, performing PET/CT in pediatric patients poses a unique challenge because children may be more vulnerable to the potential carcinogenic effects of ionizing radiation and have a higher sensitivity to developing radiation-induced malignancies [6–8]. Given these concerns, it remains prudent to eliminate unnecessary radiation exposure by investigating the optimal low-dose radiotracer activity and the short acquisition time while maintaining high diagnostic efficacy for the detection of pediatric malignancies.

Defining a standard low-count imaging protocol is a difficult task in general due to the performance differences among PET instruments [9]. Major imaging societies have proposed that the pediatric radiotracer dose regimen for 2-[^{18}F]fluoro-2-deoxy-D-glucose (FDG) PET should be within the range of 3.5-5.3 MBq/kg [10–12]. With the development of the total-body PET/CT scanner with a 194-cm-long axial field of view (FOV) [13, 14], investigations into a further reduction in the acquisition duration or injected radiotracer activity for pediatric patients can be performed. Several previous studies have used different reconstruction algorithms to simulate low-count PET images and have shown that the pediatric PET tracer dose can be reduced from 1.5 to 2.9 MBq/kg without obvious diagnostic shortcomings [15–17]. Our simulated low-count study showed that the whole-body effective dose of [^{18}F]-FDG to pediatric patients could be reduced to 0.3–0.5 mSv, suggesting an optimized regimen of 0.37 MBq/kg for 10 min/bed [18].

However, previous pediatric PET studies have focused only on theoretical extensions. There have been few studies exploring PET/CT with true low-dose injection activity, with the majority being limited to adult populations [19, 20]. Therefore, we aimed to evaluate the impact of changes to the radiotracer dose regimen on image quality and lesion detectability in pediatric patients, especially in infants and younger children. To the best of our knowledge, our study is the first to perform true low-dose pediatric PET practice and provides realistic clinical evidence. Total-body PET/CT images were obtained with a half [^{18}F]-FDG dose (1.85 MBq/kg), and different pediatric malignancies were studied. The impact of a half dose activity on image quality and diagnostic efficiency was evaluated. In addition, short acquisition times were explored using truncating list-mode PET data.

Methods

Patients

Pediatric patients who underwent total-body PET/CT using the uEXPLORER scanner (United Imaging Healthcare, Shanghai, China) with a half dose of [^{18}F]-FDG (1.85 MBq/kg) for staging or response assessments at Sun Yat-Sen University Cancer Center were retrospectively enrolled from May 2021 to December 2021. All patient diagnoses were confirmed by postoperative pathologic examination or biopsy.

The inclusion criteria were as follows: (1) younger than 18 years old and (2) actual injection regimen within the range of 1.7–2.0 MBq/kg. The exclusion criteria were as follows: (1) waiting time after [^{18}F]-FDG injection $\geq$ 80 min, (2) body mass index above the standard definition of overweight and obesity [21, 22], and (3) unevaluable background, especially for patients with diffuse infiltration or multiple metastases in the liver or spleen. The study was approved by the Institutional Review Board of Sun Yat-sen University Cancer Center, and informed consent was obtained from all patients' legal guardians.

Imaging protocol

All patients received [^{18}F]-FDG administration after fasting for 4–5 h. List-mode PET data were acquired for 600 s at 60 ± 20 min after [^{18}F]-FDG injection (1.85 ± 0.15 MBq/kg [0.05 ± 0.01 mCi/kg] activity per body weight) using a 194-cm-long axial FOV total-body PET/CT scanner (uEXPLORER, United Imaging Healthcare, Shanghai, China). Low-dose CT scans with various tube current–time products (25 to 50 mA) determined by age and body mass were obtained and reconstructed for PET attenuation correction and diagnostic purposes.

Image reconstruction

The full-time raw PET data (acquisition time of 600 s) as well as the truncated data (300 s, 180 s, 60 s, 40 s, and 20 s) were reconstructed using the ordered subset expectation maximization (OSEM) algorithm incorporating time-of-flight and point-spread function modeling (TOF-PSF) on a medical image processing workstation (uWS-MI, United Imaging Healthcare). All PET/CT images were reconstructed with a matrix of 256 × 256 and a slice thickness of 2.89 mm, producing 673 image planes per scan and resulting in a voxel size of 2.34 × 2.34 × 2.89 mm^3.

Image analysis

Objective analysis

Objective image quality evaluation was performed by an experienced technician under the supervision of a radiologist. After reviewing all pediatric oncologic patients imaged with [^{18}F]-FDG PET, different backgrounds (liver, spleen, and mediastinum) were selected because of the variability in lesions and organ uptake patterns, providing better contrast and detectability for lesions at various

positions. Spheres with diameters of 2.0 cm, 2.0 cm, and 1.5 cm were drawn on a visually homogeneous area of the right liver lobe, the spleen, and the ascending aorta (mediastinal blood pool), respectively. The location of FDG-avid lesions was confirmed on CT and PET/CT fusion images. For standard uptake value (SUV) measurements, a three-dimensional volume of interest (VOI) was drawn on axial PET images where the diameter of the lesion was maximal to ensure complete containment of the lesion. A bookmark containing the location of the VOI delineated was then propagated to the truncated acquisition group images using self-developed software in MATLAB (MathWorks, MA, USA).

Different values of semiquantitative SUV parameters, namely, SUV_{max} and SUV_{mean}, and standard deviations (SDs) were calculated for the liver, spleen, and blood pool. The signal-to-noise ratio (SNR) was analyzed to clarify the PET image quality in terms of noise level and contrast. The SNR was defined as the ratio of the SUV_{mean} to its SD in the observed region. SNR_{norm} was normalized for body mass [23, 24]. Variabilities in the lesion, SUV_{mean}, SUV_{max}, and tumor-to-back ground ratio (TBR) were also calculated. The full-time PET images served as the reference for other duration groups to evaluate lesion detectability.

Subjective evaluation

For a more comprehensive evaluation of low-count PET images, we used a combination of subjective scoring to assess image quality and lesion detection performance. Image evaluations were performed in a blinded manner using uWS-MI software (United Imaging Healthcare, SH, China). The dataset of pediatric patients was randomized and then distributed to two senior nuclear radiologists. Each patient was assigned an ID to be deanonymized later for further analysis. During the subjective scoring, series descriptions were anonymized, and the reconstructed series of each patient were randomly opened to facilitate the blind evaluation. A 5-point Likert scale was used to assess the image quality with consideration of the following parameters: (1) noise level, (2) conspicuity of suspected malignant lesions, (3) conspicuity of the liver and spleen margin, and (4) conspicuity of the bone margin. The visual scale for image quality consisted of grades 5 to 1 (Supplementary Table 1). Grade 3 indicated normal routine clinical image quality as obtained with a conventional PET/CT scanner at our center, where PET/CT scans were performed with an integrated PET/CT scanner (Biograph mCT, Siemens Healthcare, Henkestr, Germany) with an axial FOV of 16.4 cm (acquisition time 1.5–2.0 min/bed position, 6–10 bed positions/patient). Image data were acquired 60 ± 10 min after [^{18}F]-FDG injection (3.7 ± 0.37 MBq [0.1 mCi]/kg body weight).

Statistical analysis

All statistical analyses were conducted using SPSS 22.0 statistical analysis software (IBM, Armonk, NY, USA). The Kruskal–Wallis rank-sum test and Dunn's post hoc test for multiple comparisons were applied for subjective image quality analyses of different subsets. Mann–Whitney U tests were used to compare quantitative measurements between different groups. Statistical significance was set at a two-tailed $P < 0.05$.

Results

Patient characteristics

A total of one hundred pediatric patients (33 females and 67 males; mean age: 7.9 years; range: 1.0–13.2 years) with different tumors were included in this study. The characteristics of the patients are summarized in Table 1. The most prevalent diseases included lymphoma ($n = 38$), rhabdomyosarcoma ($n = 35$), neuroblastoma ($n = 15$), and Langerhans cell histiocytosis ($n = 3$). Twenty-four patients with newly diagnosed cancer underwent PET/CT for an initial assessment (lesion detection and staging), while others underwent PET/CT for recurrence detection (restaging) and therapy response assessment.

Subjective assessment of image quality

The subjective image quality was assessed with a 5-point Likert scale, and the results are summarized in Table 2.

Table 1 Clinical characteristics of pediatric oncological patients who underwent total-body PET/CT with half-dose [^{18}F]-FDG activity

Characteristic	Value ($n = 100$)
Age (years old)	7.9 ± 3.3 (range 1.0 ~ 13.2)
1 ~ 3	9
4 ~ 6	28
7 ~ 13	63
Sex	
Male	67
Female	33
BMI (kg/m^2)	15.5 ± 2.5
Injected dose (MBq)	51.0 ± 22.3
Injected dose per weight (MBq/kg)	1.85 ± 0.15
Lesion number	70
Pathological type	
Lymphoma	38
Rhabdomyosarcoma	35
Neuroblastoma	15
Langerhans cell histiocytosis	3
Germ cell tumor	2
Other diseases	7

Table 2 Subjective image quality was assessed with a 5-point Likert scale

Groups	Overall quality	Lesion conspicuity	Image noise
G600	4.9 ± 0.2	5.0 ± 0.0	4.9 ± 0.3
G300	4.9 ± 0.3	5.0 ± 0.0	4.6 ± 0.5
G180	4.4 ± 0.5	4.9 ± 0.3	4.1 ± 0.3
G60	3.5 ± 0.5	4.1 ± 0.6	3.2 ± 0.5
G40	3.0 ± 0.5	3.5 ± 0.8	2.8 ± 0.4
G20	2.0 ± 0.5	2.6 ± 0.8	1.7 ± 0.5

All data are presented as the mean ± SD

The mean and SD values of the G600 image quality scores were 4.9 ± 0.2 points for overall quality, 5.0 ± 0.0 points for lesion conspicuity and 4.9 ± 0.3 points for image noise, which demonstrated that half-dose pediatric PET imaging could meet diagnostic requirements. The overall G600, G300, G180, and G60 image quality scores were 4.9 ± 0.2, 4.9 ± 0.3, 4.4 ± 0.5, and 3.5 ± 0.5 points, respectively. All the G60 images were clinically acceptable (≥ 3 points), while 13% and 83% of the G40 and G20 images were subsequently graded as 1 and 2, respectively. The G20 image quality scores (2.0 ± 0.5 points) were significantly lower than those in the other groups (all $p < 0.05$). As shown in Fig. 1, 95% of the G600 cases and 87% of the G300 cases were evaluated as 5 points. The frequency of the overall image quality score decreased from G600 to G20, while the noise level showed the opposite trend. The noise in the images showed more variability than the overall quality or lesion conspicuity.

Lesion detectability

A total of 70 detectable lesions were included. Every location of FDG-avid lesions was confirmed on CT and PET/CT fusion images, with a total of forty-eight patients without detectable lesions in primary sites or distant metastasis. These patients were basically undergoing an interim response assessment or posttreatment assessment and surveillance. As shown in Fig. 1, 100% of the lesions identified in the half-dose images could also be clearly identified in the G60 images. In comparison, 92% and 56% of the lesions could be identified in the G40 and G20 images, respectively.

Quantitative measurement of image quality

The comparison of quantitative image quality metrics from the total-body PET/CT G600 to G20 images is shown in Fig. 2. The SUVs of both the lesion and

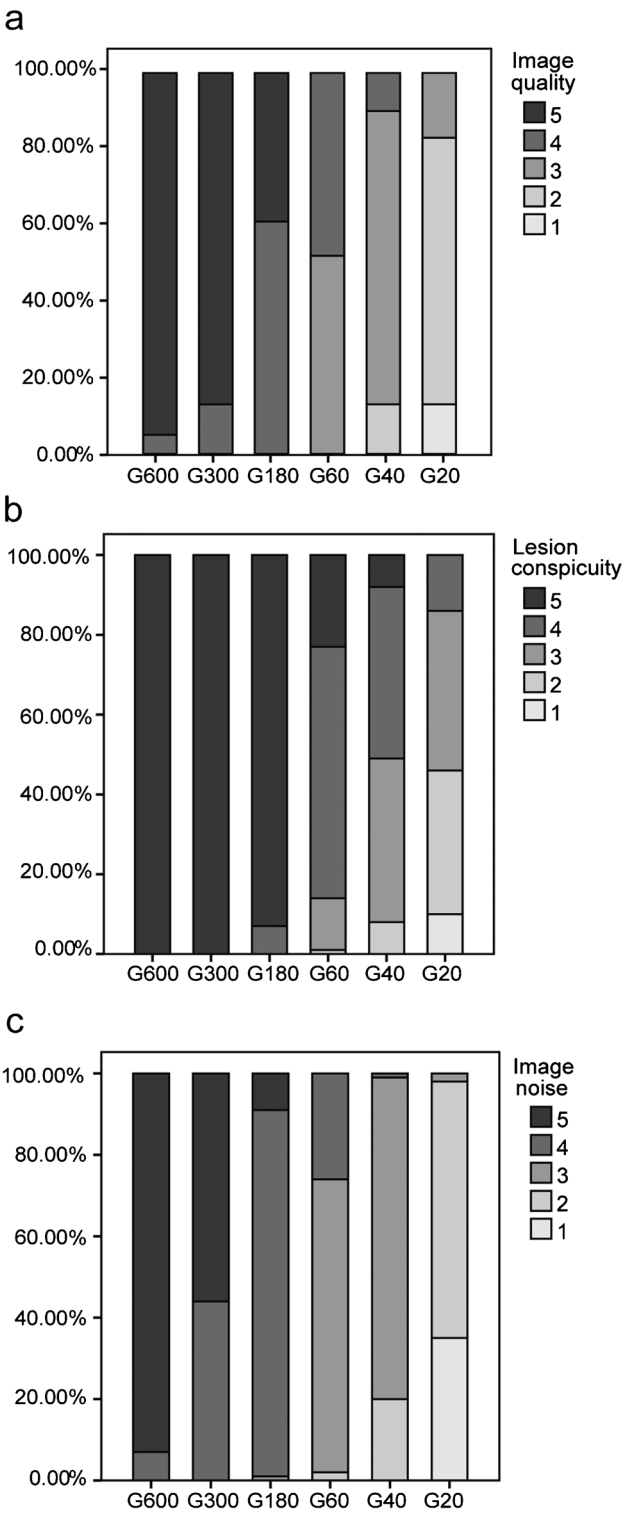

Fig. 1 The distribution of subjective three-dimensional image quality scoring among different groups. **a** Overall image quality. **b** Lesion conspicuity. **c** Image noise

background were measured to assess the change as the acquisition time was reduced. Both the SUV_{max} and SD were plotted using the average of multiple VOI measurements, along with the error bar. As shown in Table 3, in the full-time acquired PET/CT scans (600 s), the liver SUV_{max} and liver SD were 1.88 ± 0.43 and 0.09 ± 0.03, respectively, which were significantly lower than those in other short acquisition groups (all $p < 0.05$). The SUV_{max} and SD of the spleen and mediastinum showed the same trend, while the TBR values were almost the same, as shown in Fig. 2D. There was no statistically significant deviation in TBR values among all the groups, regardless of which organ was used as contrast (all $p > 0.1$). The increase in [^{18}F]-FDG uptake may be caused by age-related changes in body mass, blood volume, organ volume, and function [25, 26]. Therefore, separate evaluations according to age are warranted. The scatterplots of the SNR and SNR_{norm} with the half-dose regimen are shown in Fig. 3. None of the SNRs showed any correlation with age among the pediatric patients. In contrast, the SNR_{norm} was strongly negatively correlated with

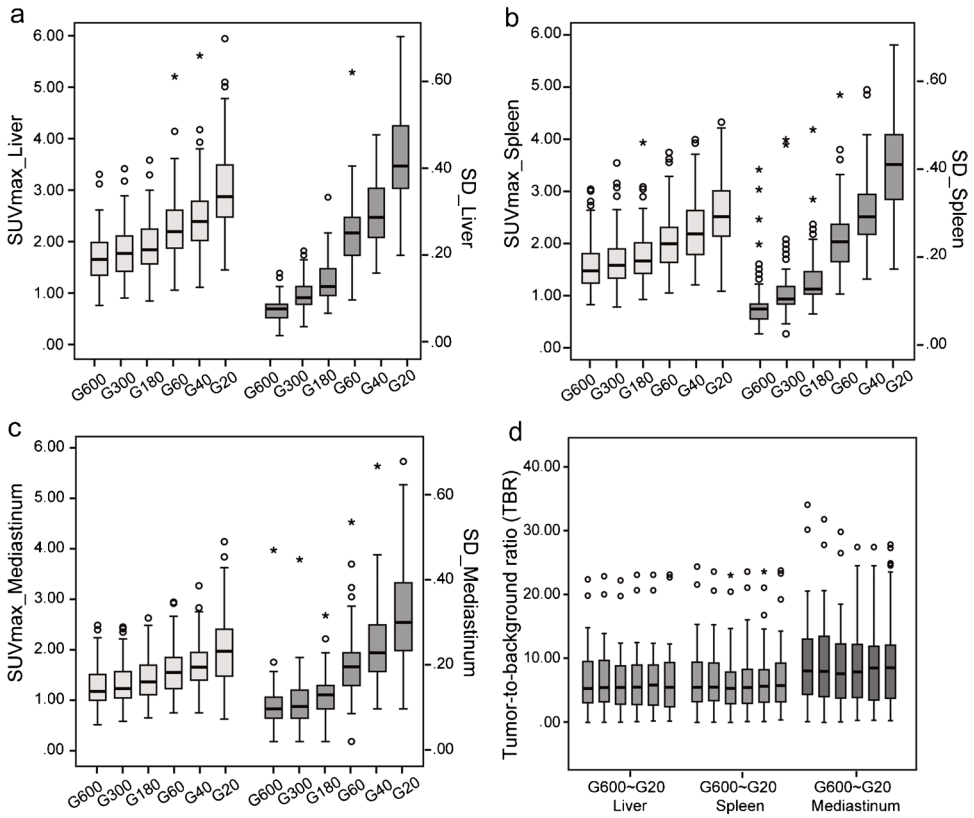

Fig. 2 The comparison of objective image quality parameters in total-body PET/CT among G600 to G20 images. **a** Liver SUV_{max} and SD. **b** Spleen SUV_{max} and SD. **c** Mediastinum SUV_{max} and SD. The SUV_{max} and SD of background parameters increased gradually as the acquisition time was reduced. The differences between each group were statistically significant ($p < 0.05$). **d** The tumor-to-background ratio (TBR) was calculated by dividing the SUV_{max} of the lesion by the SUV_{mean} of the liver, spleen and blood pool. The TBR values were almost the same. The differences were not statistically significant (all $p > 0.1$)

Table 3 SUV and SD measurement of backgrounds

	G600	G300	G180	G60	G40	G20
Liver SUV_{max}	1.88 ± 0.43	1.97 ± 0.45	2.07 ± 0.45	$2.42 \pm 0.59^{*}$	$2.63 \pm 0.61^{*}$	$3.11 \pm 0.75^{*}$
Liver SD	0.09 ± 0.03	$0.12 \pm 0.03^{*}$	$0.15 \pm 0.04^{*}$	$0.25 \pm 0.07^{*}$	$0.33 \pm 0.09^{*}$	$0.43 \pm 0.10^{*}$
Spleen SUV_{max}	1.57 ± 0.42	1.65 ± 0.45	1.72 ± 0.45	$1.97 \pm 0.49^{*}$	$2.32 \pm 0.61^{*}$	$5.51 \pm 0.66^{*}$
Spleen SD	0.09 ± 0.05	0.12 ± 0.06	$0.13 \pm 0.05^{*}$	$0.22 \pm 0.07^{*}$	$0.30 \pm 0.10^{*}$	$0.37 \pm 0.09^{*}$
Mediastinum SUV_{max}	1.32 ± 0.33	1.37 ± 0.34	1.44 ± 0.36	$1.59 \pm 0.42^{*}$	$1.67 \pm 0.38^{*}$	$2.02 \pm 0.60^{*}$
Mediastinum SD	0.1 ± 0.05	0.11 ± 0.05	$0.13 \pm 0.04^{*}$	$0.19 \pm 0.07^{*}$	$0.22 \pm 0.10^{*}$	$0.30 \pm 0.11^{*}$

All data are presented as the mean ± SD

*indicates $p < 0.05$, and G600 images serve as a quality reference

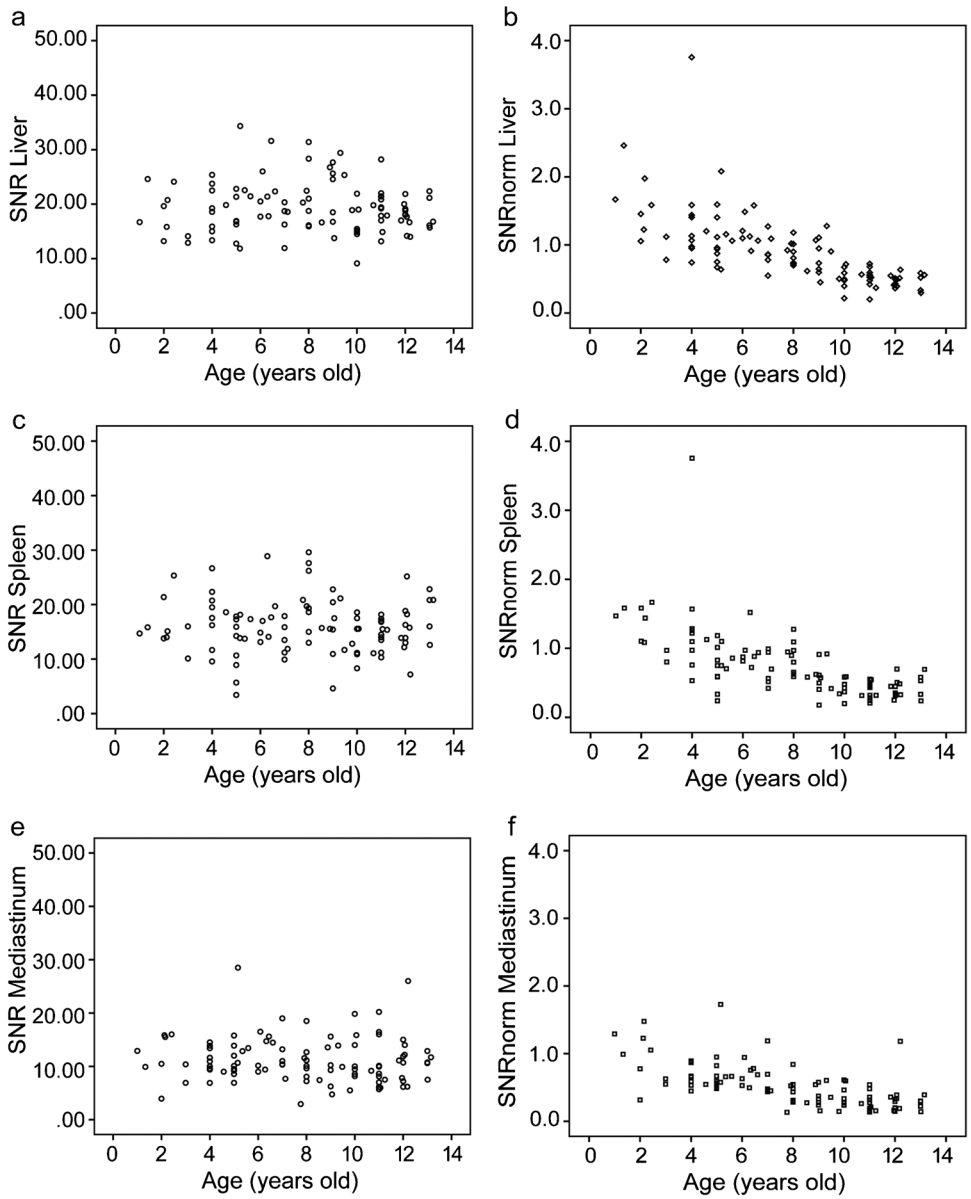

Fig. 3 Scatterplots of SNRs of the liver, spleen, mediastinum (**a**, **c**, **e**) and the SNR_{norm} of the liver, spleen, mediastinum (**b**, **d**, **f**) against age with a half-dose regimen

age (liver $r = -0.571$, spleen $r = -0.643$, mediastinum $r = -0.651$, all $p < 0.001$).

The bias and variability in lesion SUV measurements

Lesion SUV measurements are shown in Fig. 4. Using half-dose images as a reference, the G300 images showed good consistency in lesion detection. Changes in the lesion SUV_{max} showed a maximum average bias of approximately 8% for the G20 images in the pediatric patients aged 4–6 years old. Except for the G20 images, the average bias on lesion SUV_{max} was negative in almost all the other age groups. As the acquisition time was reduced from 180 to 20 s, there was a progressive increase in the variability of the lesion SUV_{max} for all age groups, with notable significance for the G20 images (all $p < 0.05$). Comparatively, the bias and variability in lesion SUV_{mean} uptake remained low as the scanning time was reduced in all age groups, showing no significance (all $p > 0.1$). In addition, the overall variability of both SUV_{max} and SUV_{mean} was minimal in infants aged 1–3 years.

Discussion

PET/CT provides both the anatomic and metabolic features of malignant tumors for clinical evaluation and has been demonstrated to be more sensitive, particularly for detecting lymph nodes, bone marrow involvement, and distant recurrent metastases, than CT alone [27, 28]. The cumulative ionizing radiation dose due to repeated scans continues to

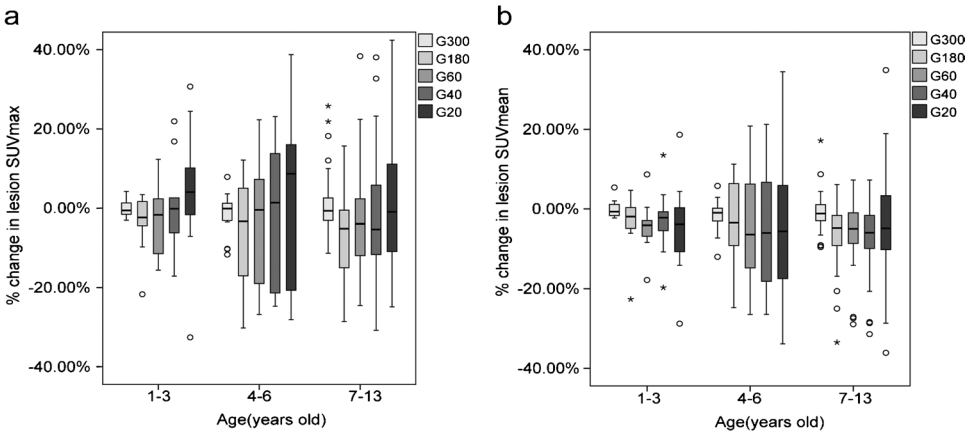

Fig. 4 The bias and variability in lesion SUV_{max} (**a**) and SUV_{mean} (**b**) for low-count PET images with different acquisition times. Data were divided into three age subgroups. The plot shows the percent changes compared with the half-dose images (G600). The total lesion count was 70

be a concern, although the relationship between exposure and radiation-related illness remains debatable [4]. Protocols for low-count [^{18}F]-FDG PET/CT based on influential imaging associations have been reported, which involve a reduction in radiotracer activity and a shortening of the acquisition time. Several studies have focused on investigating the effectivity of low-count PET imaging. Work from Liu et al. [19] has shown that a 10× reduction in injected radiotracer activity (0.37 MBq/kg) when conducting total-body dynamic [^{18}F]-FDG PET imaging shows an equivalent performance to full-activity PET imaging in healthy volunteers. Tan et al. [20] found that total-body PET/CT with half-dose [^{18}F]-FDG activity can achieve an image quality in adults that is comparable to that of conventional PET/CT.

However, pediatric patients are at a higher risk of radiation-induced cancers due to their developing bodies and longer life expectancies [29, 30]. In addition, the reported sensitivities and specificities of [^{18}F]-FDG PET/CT for tumor staging in children are over 90% [31, 32]. Few studies have concentrated on low-count PET images in pediatric patients [15–17], and most of them are only theoretical. Our study was the first to evaluate the impact of a half-dose regimen using actual rather than simulated pediatric PET imaging data. Considering the relatively small body mass of pediatric patients, the limited overall radiation exposure resulted in less benefit from true ultralow dose compared to adults. Therefore, we chose a half-dose regimen of [^{18}F]-FDG in clinical practice. Further reduction in acquisition time was performed using truncating list-mode PET data.

PET/CT image quality can be affected by multiple factors, including differences in instruments, imaging agents, waiting time, reconstruction parameters, and individual factors (including age, BMI, blood glucose level, disease history, etc.) [25, 26, 33]. To eliminate these deviations, we set relatively narrow inclusion criteria, excluding children with excessive waiting time, those receiving an insufficient or overdose delivery and those with high BMI.

The most common pediatric malignancies are mainly lymphomas, sarcomas, and neuroblastoma. Pediatric patients in various clinical disease stages were included (including newly diagnosed cancer for an initial staging, restaging, and therapy response assessment). Different backgrounds (liver, spleen, and the blood pool) were selected with consideration for the variability in lesions and organ uptake patterns and served as cutoffs for PET positivity in the evaluation of the response assessment and posttreatment surveillance [34–37]. As the liver, spleen, and mediastinum were selected for better contrast and detectability among all the pediatric patients, patients with unevaluable backgrounds, such as diffuse liver metastases that left no healthy liver background to measure, were excluded. However, VOI determination is still challenging due to large differences in age, height, and weight among children.

Our results showed that total-body PET/CT performed with a half dose (1.85 MBq/kg, estimated whole-body effective dose: 1.76–2.57 mSv) of [^{18}F]-FDG, which was much lower than previous initiatives, was feasible for clinical application in pediatric patients. The mean and SD of the G600 image quality scores were 4.9 ± 0.2 for overall quality, 5.0 ± 0.0 for lesion conspicuity, and 4.9 ± 0.3 for image noise. The image quality and lesion detectability were guaranteed and not compromised. In terms of acquisition time, a longer duration always results in better image quality. Given that the subjective downgrading of image quality was subtle as the acquisition time reduced, the increase in noise level was more prominent. Taking G600 images as a reference, the G20 image quality scores were significantly lower. Based on these clinical data, we revised our original theoretical estimations [18] and updated the recommended injection dose and acquisition time (Supplementary Table 2). A sufficient overall image quality and lesion conspicuity for clinical use could be maintained down to an acquisition time of 60 s, and none of the half-dose images were rated as undiagnostic, which was even beyond our previous estimation. For patients who may need repetitive PET/CT scans during

their disease management, lower-dose PETs could minimize overall radiation exposure. For patients who are intolerant to long-scan duration, an ultrafast scan is required with a relatively adequate dose (i.e., full dose or half dose).

The change in lesion detectability with reduced acquisition time was comparatively minimal. Figures 5 and 6 show representative views of low-count PET images. As expected, reconstructed images appeared to be noisier because of the reduced number of events in the PET list file. The subtle lesions were even clearly identifiable in the G20 images. However, our results also showed that some subtle lesions with low SUV uptake became difficult to detect in low-count images (Supplementary Fig. 2). A total of 8% and 44% of the lesions had false-negative results and could not be clearly visualized in the G40 and G20 images, indicating that they may not be feasible for clinical diagnosis and therapy response evaluations.

Consistent with previous observations [19, 38, 39], the objective analyses showed that there was a pronounced increase in background SUV_{max} and SD as the acquisition time was reduced. The same tendency was demonstrated across all three backgrounds, which means that a short acquisition time might diminish the accuracy of SUV measurements. This increase may be caused by noise amplification, therefore resulting in a higher maximum pixel value in the background measurement. There was no statistically significant deviation in TBR values as the acquisition time systematically reduced, which indicated good maintenance in lesion conspicuity.

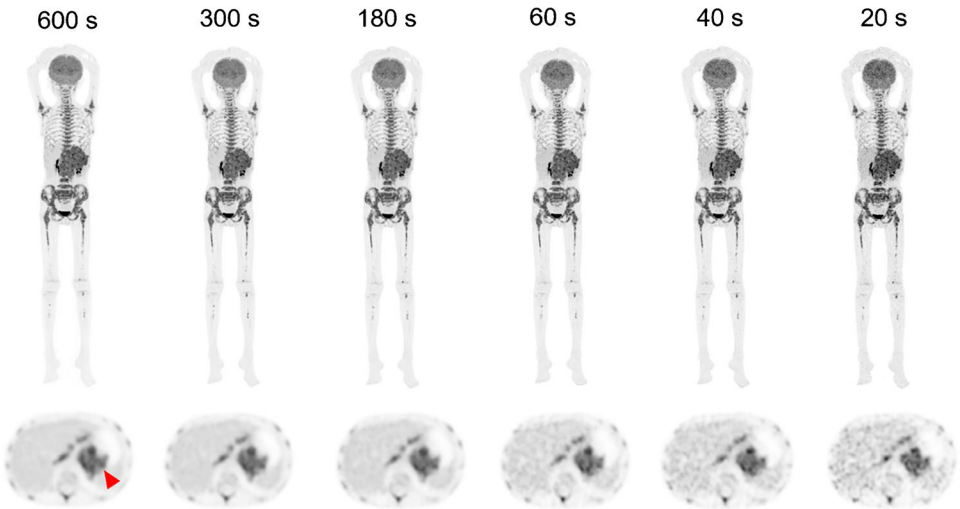

Fig. 5 An 11-year-old child with neuroblastoma confirmed by subsequent surgery. The maximum intensity projection (MIP) and axial images of the avid-FDG lesion in the retroperitoneum (red arrow) were identified. The serial low-count PET images were generated by shortening the length of frame duration used for reconstruction. The overall image quality scores of the G600 to G20 images were 5, 5, 4, 3, 3, and 2 points, respectively. The lesion was even identifiable at an acquisition time of 20 s

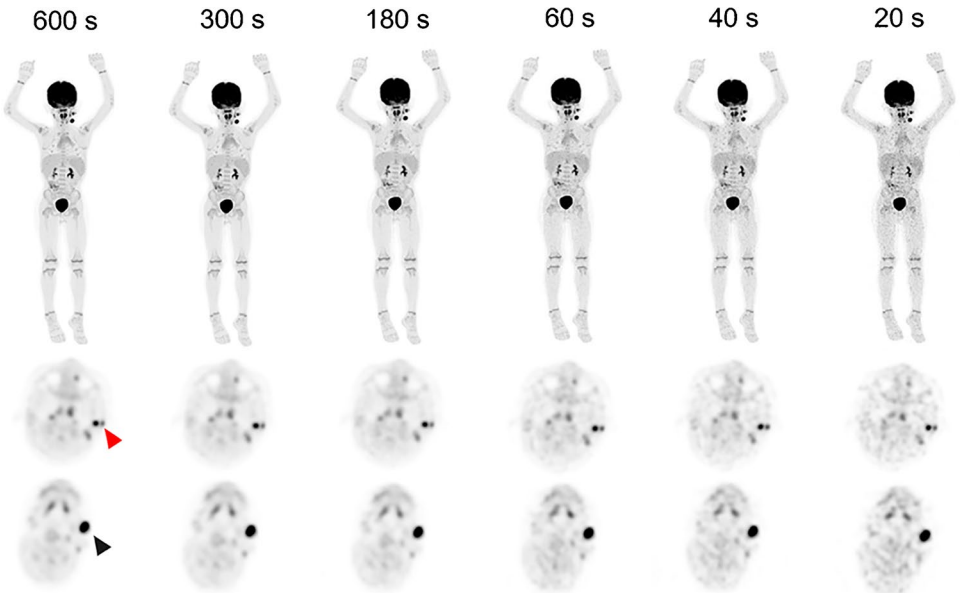

Fig. 6 A 4-year-old child with Burkitt lymphoma confirmed by biopsy. Clinical half-dose and generated low-count images are shown. The axial images showed lesions in the left parotid area (red arrow) and the left submandibular area (black arrow). Noise was visibly increased with a reduction in acquisition time. Subtle [.^{18}F]-FDG–avid lesion detection within the left parotid area was uncompromised even at 20 s

One of the significant challenges in pediatric low-count PET images is the considerable variation in patient age, resulting in different body sizes and metabolic patterns, which may impact dosimetry measurements [40–42]. Therefore, separate evaluations are warranted according to age. Our study was based on PET data from patients ranging from 1.0 to 13.2 years old. Therefore, the age-dependent pharmacokinetics of [^{18}F]-FDG were directly included. In particular, infants with more distinct characteristics were involved. The SNR had almost no correlation with age, which means that the current half-dose regimen already provides a constant image quality across the patient population. Younger children showed high SNR_{norm} values, which was probably caused by less attenuation and scatter due to their lower body mass. In addition, Fig. 4 shows that the overall variability in both lesion SUV_{max} and SUV_{mean} was minimal in infants aged 1–3 years, which corroborated the same conclusion as Fig. 3, indicating that for younger patients, less injection activity was needed to obtain optimal image quality. The acquisition time or dosage regimen can be further reduced in younger patients, alleviating concerns related to repeated PET/CT.

As shown in Fig. 4, the G300 images showed high consistency in both lesion SUV_{max} and SUV_{mean} compared to the half-dose images. The variability in lesion SUV_{max} gradually increased as the time was reduced and was generally lower than 20%, similar to previous studies [43, 44]. The average bias in lesion SUV_{max} was negative in almost all other age groups except for G20, which was probably due to the higher noise level in the G20 images. This observation also indicated unstable SUV_{max} values in low-count images. Comparatively, the lesion SUV_{mean} showed less bias and variability as the time was reduced, suggesting that SUV_{mean} may act as a much more accurate and stable metric in low-count images.

Our study has several potential limitations. First, it was a single-center study, and [^{18}F]-FDG PET/CT images were obtained from a specific scanner. Therefore, they may not be generalizable to other centers, other PET equipment, or tracers beyond FDG. Second, pediatric patients at our center were restricted to only certain common malignancies, such as lymphomas, sarcomas, and neuroblastoma. Patients of the exclusion criteria were not involved in the study. These might result in selection bias. Third, the anonymized low-count PET series for each patient were reviewed simultaneously, which may increase the conspicuity of some subtle lesions. Furthermore, we did not use disease subgroups because of the relatively small population of patients with different tumor types and disease stages.

Conclusions

Our study demonstrated that total-body PET/CT using a true half dose of [^{18}F]-FDG could meet the needs of clinical diagnosis. In addition, sufficient image quality and lesion conspicuity could be achieved at a short acquisition time of 60 s with half-dose activity. For pediatric patients undergoing repetitive PET/CT scans during their disease management, lower-dose PET scans could minimize the overall radiation exposure. For patients who are intolerant of a long scan duration, ultrafast scanning is recommended with a relatively adequate dose. This optimization will serve as a novel reference for further pediatric PET dose investigations and lead to more efficient PET/CT scans while maintaining high clinical value.

Supplementary Information The online version contains supplementary material available at https://doi.org/10.1007/s00259-022-05893-8.

Author contribution Conceptualization: Yingying Hu, Yizhuo Zhang, and Yumo Zhao; methodology: Wanqi Chen, Lei Liu, Yumo Zhao, and Zhijian Li; formal analysis and investigation: Yingying Hu, Wanqi Chen, Lei Liu, Zhijian Li, and Weiguang Zhang; writing—original draft preparation: Wanqi Chen, Lei Liu, and Yingying Hu; writing—review and editing: Yingying Hu, Yizhuo Zhang, Yumo Zhao, Runze Wu, Yinghe Li, Shatong Li, and Xu Zhang; technical support: Hongyan Sun, Debin Hu, Runze Wu and Yun Zhou; resources: Yingying Hu; and supervision: Yumo Zhao, Yizhuo Zhang, and Yingying Hu. All authors read and approved the final manuscript.

Data availability The datasets generated during and/or analyzed during the current study are available from the corresponding author upon reasonable request.

Code availability The code applied during and/or analyzed during the current study is available from the corresponding author upon reasonable request.

Declarations

Ethics approval All procedures performed in studies involving human participants were conducted in accordance with the ethical standards of the institutional and/or national research committee and with the 1964 Declaration of Helsinki and its later amendments or comparable ethical standards.

Consent to participate Informed consent was obtained from legal guardians.

Consent for publication Additional informed consent was obtained from all legal guardians for whom identifying information is included in this article.

Conflict of interest Authors Runze Wu, Hongyan Sun, Debin Hu, and Yun Zhou are employees of United Imaging Research. The other authors working at Sun Yat-sen University Cancer Center have full control of the data and declare that they have no conflicts of interest.

References

1. Boellaard RD-BR, Oyen WJ, Giammarile F, Tatsch K, Eschner W, et al. European Association of Nuclear Medicine (EANM). FDG PET/CT: EANM procedure guidelines for tumour imaging: version 2.0. Eur J Nucl Med Mol Imaging. 2015;42:28–54. https://doi.org/10.1007/s00259-014-2961-x.
2. Fahey FHTS, Adelstein SJ. Minimizing and communicating radiation risk in pediatric nuclear medicine. J Nucl Med. 2011;52:1240–51. https://doi.org/10.2967/jnumed.109.069609.
3. Ricard F, Cimarelli S, Deshayes E, Mognetti T, Thiesse P, Giammarile F. Additional benefit of F-18 FDG PET/CT in the staging and follow-up of pediatric rhabdomyosarcoma. Clin Nucl Med. 2011;36:672–7. https://doi.org/10.1097/RLU.0b013e318217ae2e.
4. Fahey FH, Goodkind A, MacDougall RD, Oberg L, Ziniel SI, Cappock R, et al. Operational and dosimetric aspects of pediatric PET/CT. J Nucl Med. 2017;58:1360–6. https://doi.org/10.2967/jnumed.116.182899.
5. Turpin S, Martineau P, Levasseur MA, Meijer I, Décarie JC, Barsalou J, et al. 18F-Flurodeoxyglucose positron emission tomography with computed tomography (FDG PET/CT) findings in children with encephalitis and comparison to conventional imaging. Eur J Nucl Med Mol Imaging. 2019;46:1309–24. https://doi.org/10.1007/s00259-019-04302-x.
6. Chawla SC, Federman N, Zhang D, Nagata K, Nuthakki S, McNitt-Gray M, et al. Estimated cumulative radiation dose from PET/CT in children with malignancies: a 5-year retrospective review. Pediatr Radiol. 2010;40:681–6. https://doi.org/10.1007/s00247-009-1434-z.
7. Mercolini F, Zucchetta P, Jehanno N, Corradini N, Van Rijn RR, Rogers T, et al. Role of (18)F-FDG-PET/CT in the staging of metastatic rhabdomyosarcoma: a report from the European paediatric Soft tissue sarcoma Study Group. Eur J cancer (Oxford, England: 1990). 2021;155:155–62. https://doi.org/10.1016/j.ejca.2021.07.006.
8. Nievelstein RA, Quarlesvanufford HM, Kwee TC, Bierings MB, Ludwig I, Beek FJ, et al. Radiation exposure and mortality risk from CT and PET imaging of patients with malignant lymphoma. Eur Radiol. 2012;22:1946–54. https://doi.org/10.1007/s00330-012-2447-9.
9. Alessio AM, Farrell MB, Fahey FH. Role of reference levels in nuclear medicine: a report of the SNMMI Dose Optimization Task Force. J Nucl Med. 2015;56:1960–4. https://doi.org/10.2967/jnumed.115.160861.
10. Poli GL, Torres L, Coca M, Veselinovic M, Lassmann M, Delis H, et al. Paediatric nuclear medicine practice: an international survey by the IAEA. Eur J Nucl Med Mol Imaging. 2020;47:1552–63. https://doi.org/10.1007/s00259-019-04624-w.
11. Treves ST, Gelfand MJ, Fahey FH, Parisi MT. 2016 Update of the North American Consensus Guidelines for Pediatric Administered Radiopharmaceutical Activities. J Nucl Med. 2016;57:15n-n18.
12. Lassmann M, Biassoni L, Monsieurs M, Franzius C. The new EANM paediatric dosage card: additional notes with respect to F-18. Eur J Nucl Med Mol Imaging. 2008;35:1666–8. https://doi.org/10.1007/s00259-008-0799-9.
13. Cherry SR, Jones T, Karp JS, Qi J, Moses WW, Badawi RD. Total-body PET: maximizing sensitivity to create new opportunities for clinical research and patient care. J Nucl Med. 2018;59:3–12. https://doi.org/10.2967/jnumed.116.184028.
14. Badawi RD, Shi H, Hu P, Chen S, Xu T, Price PM, et al. First human imaging studies with the EXPLORER total-body PET scanner. J Nucl Med. 2019;60:299–303. https://doi.org/10.2967/jnumed.119.226498.
15. Schmall JP, Surti S, Otero HJ, Servaes S, Karp JS, States LJ. Investigating low-dose image quality in whole-body pediatric (18)F-FDG scans using time-of-flight PET/MRI. J Nucl Med. 2021;62:123–30. https://doi.org/10.2967/jnumed.119.240127.
16. Gatidis S, Schmidt H, la Fougère C, Nikolaou K, Schwenzer NF, Schäfer JF. Defining optimal tracer activities in pediatric oncologic whole-body (18)F-FDG-PET/MRI. Eur J Nucl Med Mol Imaging. 2016;43:2283–9. https://doi.org/10.1007/s00259-016-3503-5.
17. Kertész H, Beyer T, London K, Saleh H, Chung D, Rausch I, Cal-Gonzalez J, Kitsos T, Kench PL. Reducing radiation exposure to paediatric patients undergoing [18F]FDG-PET/CT imaging. Mol Imaging Biol. 2021 ;23(5):775–86. https://doi.org/10.1007/s11307-021-01601-4.
18. Zhao YM, Li YH, Chen T, Zhang WG, Wang LH, Feng J, et al. Image quality and lesion detectability in low-dose pediatric (18)F-FDG scans using total-body PET/CT. Eur J Nucl Med Mol Imaging. 2021;48:3378–85. https://doi.org/10.1007/s00259-021-05304-4.
19. Liu G, Hu P, Yu H, Tan H, Zhang Y, Yin H, et al. Ultra-low-activity total-body dynamic PET imaging allows equal performance to full-activity PET imaging for investigating kinetic metrics of (18)F-FDG in healthy volunteers. Eur J Nucl Med Mol Imaging. 2021;48:2373–83. https://doi.org/10.1007/s00259-020-05173-3.
20. Tan H, Sui X, Yin H, Yu H, Gu Y, Chen S, et al. Total-body PET/CT using half-dose FDG and compared with conventional PET/CT using full-dose FDG in lung cancer. Eur J Nucl Med Mol Imaging. 2021;48:1966–75. https://doi.org/10.1007/s00259-020-05091-4.
21. Spinelli A, Buoncristiano M, Nardone P, Starc G, Hejgaard T, Júlíusson PB, et al. Thinness, overweight, and obesity in 6- to 9-year-old children from 36 countries: The World Health Organization European Childhood Obesity Surveillance Initiative-COSI 2015–2017. Obesity Rev. 2021;22(Suppl 6):e13214. https://doi.org/10.1111/obr.13214.
22. Daniels SR, Arnett DK, Eckel RH, Gidding SS, Hayman LL, Kumanyika S, et al. Overweight in children and adolescents: pathophysiology, consequences, prevention, and treatment. Circulation. 2005;111:1999–2012. https://doi.org/10.1161/01.Cir.0000161369.71722.10.
23. de Groot EH, Post N, Boellaard R, Wagenaar NR, Willemsen AT, van Dalen JA. Optimized dose regimen for whole-body FDG-PET imaging. EJNMMI Res. 2013;3:63. https://doi.org/10.1186/2191-219x-3-63.
24. Cox CPW, van Assema DME, Verburg FA, Brabander T, Konijnenberg M, Segbers M. A dedicated paediatric [(18)F]FDG PET/CT dosage regimen. EJNMMI Res. 2021;11:65. https://doi.org/10.1186/s13550-021-00812-8.
25. Meier JM, Alavi A, Iruvuri S, Alzeair S, Parker R, Houseni M, et al. Assessment of age-related changes in abdominal organ structure and function with computed tomography and positron emission tomography. Semin Nucl Med. 2007;37:154–72. https://doi.org/10.1053/j.semnuclmed.2007.02.001.
26. Yeung HW, Sanches A, Squire OD, Macapinlac HA, Larson SM, Erdi YE. Standardized uptake value in pediatric patients: an investigation to determine the optimum measurement parameter. Eur J Nucl Med Mol Imaging. 2002;29:61–6. https://doi.org/10.1007/s00259-001-0662-8.
27. Wegner EA, Barrington SF, Kingston JE, Robinson RO, Ferner RE, Taj M, et al. The impact of PET scanning on management of paediatric oncology patients. Eur J Nucl Med Mol Imaging. 2005;32:23–30. https://doi.org/10.1007/s00259-004-1645-3.
28. Montravers F, McNamara D, Landman-Parker J, Grahek D, Kerrou K, Younsi N, et al. [(18)F]FDG in childhood lymphoma: clinical utility and impact on management. Eur J Nucl Med Mol Imaging. 2002;29:1155–65. https://doi.org/10.1007/s00259-002-0861-y.
29. Sgouros G, Frey EC, Bolch WE, Wayson MB, Abadia AF, Treves ST. An approach for balancing diagnostic image quality with

cancer risk: application to pediatric diagnostic imaging of 99mTc-dimercaptosuccinic acid. J Nucl Med. 2011;52:1923–9. https://doi.org/10.2967/jnumed.111.092221.
30. Alessio AM, Sammer M, Phillips GS, Manchanda V, Mohr BC, Parisi MT. Evaluation of optimal acquisition duration or injected activity for pediatric 18F-FDG PET/CT. J Nucl Med. 2011;52:1028–34. https://doi.org/10.2967/jnumed.110.086579.
31. Tatsumi M, Miller JH, Wahl RL. 18F-FDG PET/CT in evaluating non-CNS pediatric malignancies. J Nucl Med. 2007;48:1923–31. https://doi.org/10.2967/jnumed.107.044628.
32. Uslu L, Donig J, Link M, Rosenberg J, Quon A, Daldrup-Link HE. Value of 18F-FDG PET and PET/CT for evaluation of pediatric malignancies. J Nucl Med. 2015;56:274–86. https://doi.org/10.2967/jnumed.114.146290.
33. Büsing KA, Schönberg SO, Brade J, Wasser K. Impact of blood glucose, diabetes, insulin, and obesity on standardized uptake values in tumors and healthy organs on 18F-FDG PET/CT. Nucl Med Biol. 2013;40:206–13. https://doi.org/10.1016/j.nucmedbio.2012.10.014.
34. Sastre J, Pallardó FV, Plá R, Pellín A, Juan G, O'Connor JE, et al. Aging of the liver: age-associated mitochondrial damage in intact hepatocytes. Hepatology (Baltimore, MD). 1996;24:1199–205. https://doi.org/10.1002/hep.510240536.
35. Schmidkonz C, Krumbholz M, Atzinger A, Cordes M, Goetz TI, Prante O, et al. Assessment of treatment responses in children and adolescents with Ewing sarcoma with metabolic tumor parameters derived from (18)F-FDG-PET/CT and circulating tumor DNA. Eur J Nucl Med Mol Imaging. 2020;47:1564–75. https://doi.org/10.1007/s00259-019-04649-1.
36. Pijl JP, Kwee TC, Slart R, Yakar D, Wouthuyzen-Bakker M, Glaudemans A. Clinical implications of increased uptake in bone marrow and spleen on FDG-PET in patients with bacteremia. Eur J Nucl Med Mol Imaging. 2021;48:1467–77. https://doi.org/10.1007/s00259-020-05071-8.
37. Patel NH, Osborne MT, Teague H, Parel P, Svirydava M, Sorokin AV, et al. Heightened splenic and bone marrow uptake of (18)F-FDG PET/CT is associated with systemic inflammation and subclinical atherosclerosis by CCTA in psoriasis: An observational study. Atherosclerosis. 2021;339:20–6. https://doi.org/10.1016/j.atherosclerosis.2021.11.008.
38. Akamatsu G, Ishikawa K, Mitsumoto K, Taniguchi T, Ohya N, Baba S, et al. Improvement in PET/CT image quality with a combination of point-spread function and time-of-flight in relation to reconstruction parameters. J Nucl Med. 2012;53:1716–22. https://doi.org/10.2967/jnumed.112.103861.
39. Zhang YQ, Hu PC, Wu RZ, Gu YS, Chen SG, Yu HJ, et al. The image quality, lesion detectability, and acquisition time of (18)F-FDG total-body PET/CT in oncological patients. Eur J Nucl Med Mol Imaging. 2020;47:2507–15. https://doi.org/10.1007/s00259-020-04823-w.
40. Shammas A, Lim R, Charron M. Pediatric FDG PET/CT: physiologic uptake, normal variants, and benign conditions. Radiographics. 2009;29:1467–86. https://doi.org/10.1148/rg.295085247.
41. Halpern BS, Dahlbom M, Quon A, Schiepers C, Waldherr C, Silverman DH, et al. Impact of patient weight and emission scan duration on PET/CT image quality and lesion detectability. J Nucl Med. 2004;45:797–801.
42. Accorsi R, Karp JS, Surti S. Improved dose regimen in pediatric PET. J Nucl Med. 2010;51:293–300. https://doi.org/10.2967/jnumed.109.066332.
43. de Langen AJ, Vincent A, Velasquez LM, van Tinteren H, Boellaard R, Shankar LK, et al. Repeatability of 18F-FDG uptake measurements in tumors: a metaanalysis. J Nucl Med. 2012;53:701–8. https://doi.org/10.2967/jnumed.111.095299.
44. Wahl RL, Jacene H, Kasamon Y, Lodge MA. From RECIST to PERCIST: evolving considerations for PET response criteria in solid tumors. J Nucl Med. 2009;50(Suppl 1):122s-s150. https://doi.org/10.2967/jnumed.108.057307.